COMPREHENSIVE STUDY OF A PROPORTIONAL CHAMBER CATHODE'S SURFACE AFTER ITS OPERATION IN AN EXPERIMENT AT THE LARGE HADRON COLLIDER

G.E. Gavrilov, A.A. Dzyuba, O.E. Maev

1. Introduction

Radiation resistance of multiwire proportional chambers (MWPCs) in experiments at the Large Hadron Collider (LHC) remains a hot topic, due to the recent tenfold increase in the luminosity of the collider after its upgrading. The key motivation for this research is to maintain the stability of MWPCs for the next 10 years of the LHC operation with an expected jump in the ionization current and the already observed spontaneous self-sustaining current – Malter effect (ME) [1]. Spontaneous currents arising in MWPCs are ten times higher than the current from collisions of the proton beams in the collider and reach up to 30–40 μA [2]. This complicates operation of the readout electronics and overloads it with false responses. The ME current localized at a point on the cathode as well accelerates the aging of the anode wires located nearby.

It should be noted that the main source of the background in the muon detector of the LHCb experiment are fast neutrons with energies of up to several hundred MeV. They form photons with energies of 0.1–1 MeV as a result of nuclear interaction with the structural materials of the facility. Compton electrons are generated when photons pass through the gas volume of the MWPC, and their energy exceeds the threshold of the formation of radiation defects in metals ~ 0.5 MeV [3, 4].

The aim of studying the surface of the cathode of the MWPC was to determine the cause of ME currents in order to develop non-invasive ways of suppressing them.

2. Experiment

A module of the MWPCs of the muon detector of the LHCb experiment (type M5R4_FIR037), which operated at the LHC ($T \approx 3.2 \cdot 10^7$ s), was chosen for the study [2]. This module consists of four detecting planes (Gaps A, B, C and D) of MWPCs, and only Gap D's plane regularly displays spontaneous self-sustaining currents. It was from this plane that cathode samples were taken (disks 1 mm thick with radius of 23 mm).

As a result of the LHC operation with a working gas mixture of $Ar\ 40\% / CO_2\ 55\% / CF_4\ 5\%$, the MWPC anode wires in the M5R4_FIR037 module accumulated charges of $Q \approx 1\ mC \cdot cm^{-1}$ (or ~ 2.5 $mC \cdot cm^{-2}$). After the module was dismantled from the muon detector, it was additionally studied at the gamma irradiation facility (GIF++) [5] using an $Ar\ 40\% / CO_2\ 58\% / CF_4\ 2\%$ gas mixture. As a result, a charge of $Q_1 \approx 0.5\ mC \cdot cm^{-1}$ was additionally accumulated on the wires.

It should be noted that the charge Q_1 accumulated in a very short time (the current of the MWPC detecting planes was two orders of magnitude higher than that during operation as a part of the muon detector). The CF_4 content in the working mixture was 2% and the gas flow through the volume was reduced by 30%. Despite the tougher testing conditions, there were no new zones of spontaneous electron emission in the MWPCs. The already existing ME zone remained in its original place.

High voltage was not applied to one of the MWPC planes (Gap A) during operation on the collider (and at the facility). Like its counterparts, however, this plane was exposed to charged particles with an intensity of $R \approx 350\ Hz \cdot cm^{-2}$. Since there was no electric field, the cathodes in the Gap A plane were not exposed to the plasma chemical effect of products of the dissociation of the gas mixture's components. The samples taken on this plane are therefore referred to below as control samples. They were compared to samples from the Gap D plane, which had experienced the entire set of radiation and plasma chemical effects. The characteristic fluence of minimum ionizing particles for the MWPC planes was $F \approx 5 \cdot 10^{13}\ cm^{-2}$. The dose on the copper foil of the cathode (35 μm thick), calculated using the GEANT4 software package, was thus at a level of $D \approx 1.3$ Gy.

The count rates of Gap D anode wires combined into groups were measured to localize the zone of the ME current generation in the MWPCs during irradiation at the GIF++ facility. The zone of generation was

therefore found as a group of wires with a very high count rate. Here and below, the cathode samples taken along these wires are referred to as ME samples, while those taken outside the zone of the high count rate are non-ME samples.

Figure 1 (*upper part*) shows photographs of the M5R4_FIR037 cathode planes after disassembly. Photos of the Gap A and Gap D planes are on the left. The layout of the samples on the cathode is on the right. ME samples were taken in series along the *Y* axis (30 cm long) parallel to the anode wires with the highest count rate. Non-ME samples were also taken along the *Y* axis, but were offset by ~ 20 cm from the zone of spontaneous currents. Visual inspection of the MWPC module after disassembly showed that the cathodes of all the MWPC planes, except for the Gap A plane, were strongly oxidized (the *lower photo* of Fig. 1). However, since the ME was observed only on the Gap D plane, we can assume that the oxidation and reduction of copper are still not sufficient reasons for the emission currents on the cathode [6, 7], although it is known, that the island oxidation of copper surface with the formation of Cu_2O often leads to the emission currents in an electric field of $E \geq 50$ kV · cm^{-1} [8].

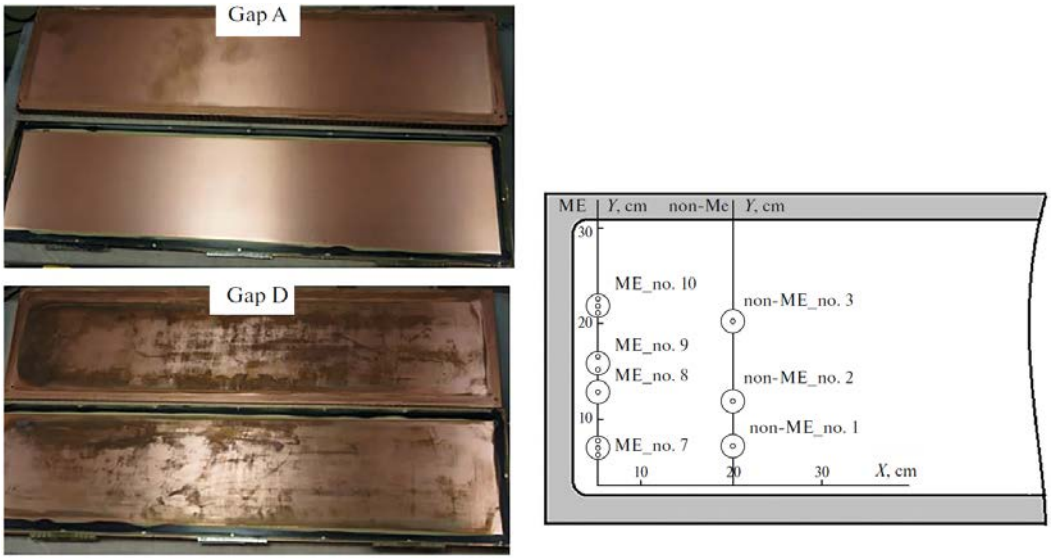

Fig. 1. Photos of the cathode planes Gap A and Gap D after the disassembly of the MWPC (*left*); the arrangement of samples (*dots*) on the cathode (*right*)

The surface morphology of the cathode samples was studied by atomic force microscopy (AFM) with Solver Next scanning probe microscope (OAO NT-MDT, Zelenograd, Russia). Surfaces were scanned by NSG10/TiN cantilevers in the tapping (topography and phase) and contact (current spectroscopy at air under normal conditions) modes. Elemental analysis of the samples surfaces was performed *via* Rutherford backscattering spectroscopy (RBS) on the Mikrozond component of the Mikrozond-EGP-10 complex at a beam energy of 4 MeV, a proton current 0.01 nA on the samples, and a beam size of 30 × 30 μm^2. The scanning area was 300 × 300 μm^2. The phase composition of samples was determined using a Shimadzu XRD-7000 *X*-ray diffractometer and copper anode radiation (wavelength, 1.542 A), $V = 40$ kV, $I = 30$ mA.

The composition of microparticles and microstructured objects was analysed *via* Raman spectroscopy. A RamMics M532R Raman microscope was used that combined the capabilities of an EnSpectr R532R Scientific Edition Raman analyser and an Olympus CX-41 microscope.

3. Results and discussion

An analysis of the surface structure of samples taken from different sections of the cathode in the Gap D plane showed the nonuniformity of the radiation aging processes. Figure 2*a* (*upper part*) shows a scan of the surface of a control sample (Gap A plane). Figures 2*b, c* show scans of no-ME samples 2 and 3 (Gap D plane). The surface of the control sample has a weakly structured fibrous relief with zones of disorder

(technological defects) and single peaks. Primary defects most likely were formed on the cathode when bonding copper foils to fiberglass plates during production.

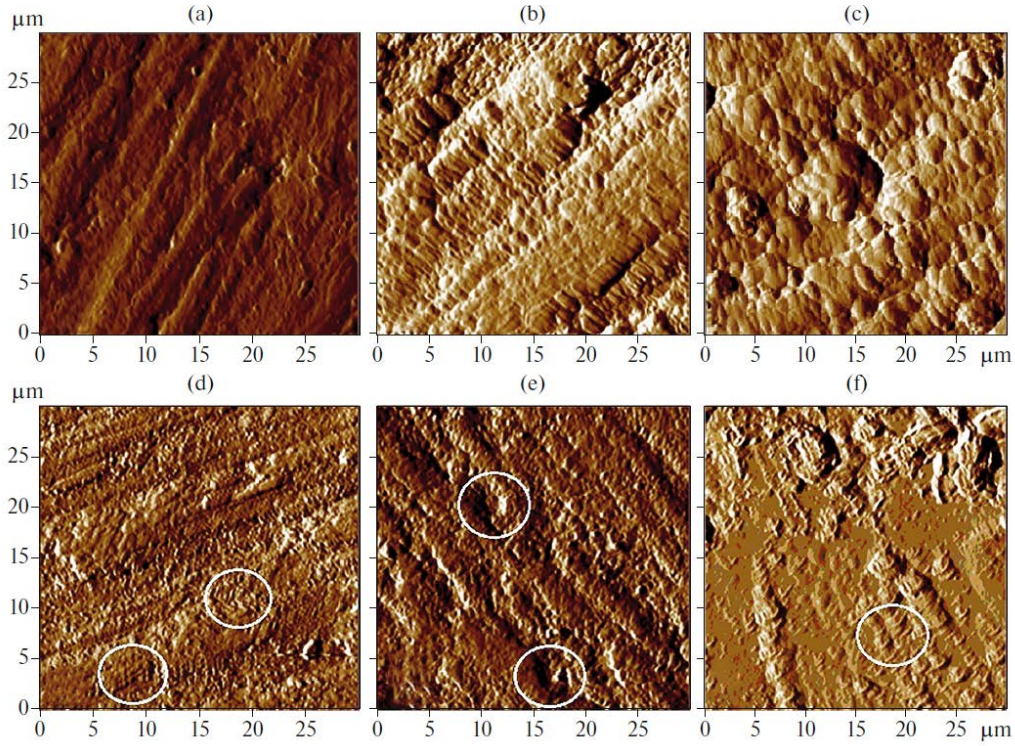

Fig. 2. Atomic force microscopy scan of the sample surface with a scanning field size of 30 × 30 μm^2: *a* – control sample; *b* – non-ME 1; *c* – non-ME 2; *d* – ME 5; *e* – ME 8; *f* – ME 10

In addition to radiation, the surfaces of ME and non-ME samples were exposed to products of the dissociative ionization of gas molecules (O·, F·, CF_n· and CO· radicals, where · is the number of not coupled electrons of the outer shell) in vicinity of the anode wires of the MWPC [9]. Thus, a different morphological type of surface (terraced structures with isolated cells) was formed on the cathodes than on the control sample. As can be seen in Figs. 2*b*, *c*, non-ME samples were characterized by zones of segregation in addition to terraced structures.

Figures 2*d–f* (*lower parts*) show AFM scans of ME samples 5, 8 and 10. Most of their surface areas were subjected to erosion. Common to these samples are terraced structures similar to those found in non-ME samples (marked with white ovals in Figs. 2*d–f*). Changes in the surface morphology of ME samples were due to such radiation defects as blisters, craters, and finely dispersed structures characteristic of copper oxide Cu_2O. These structures are clearly visible in Figs. 2*d*, *e*. Both the foamy areas on the surface (see Fig. 2*d*) due to small blisters and the formation of craters caused by radiation (see Fig. 2*e*) do not have melting zones.

Zones of structural phase transitions (oxidation and melting) are clearly visible in Fig. 2*f*. The observed smoothing due to melting is distributed over image area of 30 × 30 μm^2, due apparently to the thermal action of high-density emission currents on the cathode copper foil. Surface melting can also occur in the copper foil along the trajectories of fast charged particles, which cause cascades and subcascades of moving vacancies and interstitial atoms. However, such effects at a relatively low intensity of irradiation ($R \approx 350$ Hz · cm^{-2}) should be point-localized [10].

At the same time, due to absorption by copper from the gas mixture of molecules containing oxygen, carbon and fluorine, the islands of dielectric oxide Cu_2O grow [2, 8] and nanocarbon and fluorocarbon films form [11, 12] on the cathode surface. The point emission of electrons is possible for such formations under the action of an electric field, which can heat their surfaces to the melting point. The inhomogeneity of the

distribution of emission points on the cathode could be due to the turbulence of the gas flow in the narrow gaps of the MWPC (5 mm) near the inlet and outlet of the gas mixture [2].

Figure 3 presents results of an analysis of the main characteristics of the surfaces of samples (roughness S and peak height differences Δh, both in nm). Data for four ME samples and three non-ME samples are given that depend on their coordinates along the Y axis. The surfaces of ME samples 7, 9 and 10 ($Y \approx 6$ cm, $Y \approx 15$ cm and $Y \approx 32$ cm, respectively) were examined at several points.

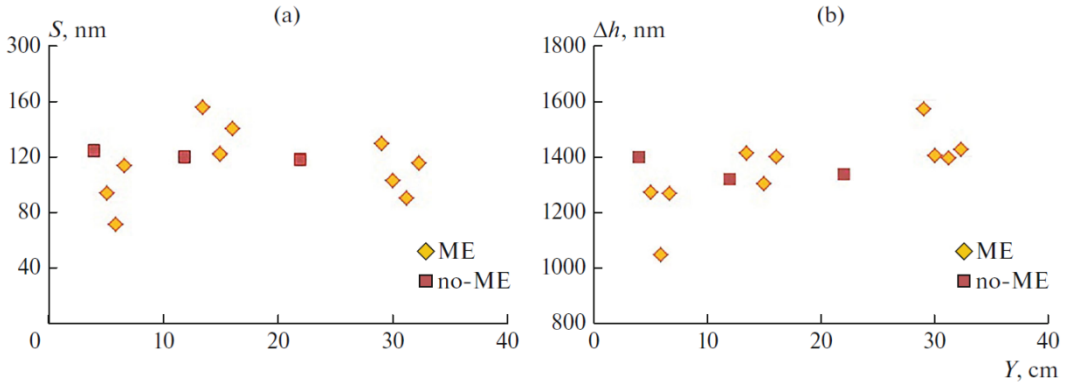

Fig. 3. Distribution of (*a*) roughness S and (*b*) peak heights Δh on the surface of ME samples and non-ME samples along the Y axes in and outside the zone of spontaneous currents

The roughness of the control sample surface was $S \approx 90$–100 nm, and the difference between peak heights at different points was $\Delta h \approx 1\,100$–$1\,200$ nm, very close to the values in Fig. 3. The surface is rougher than that on the control sample in the zones on the Gap D plane, regardless of electron emission. The roughness varies in the range of $S \approx 100$–140 nm, and the difference between peak heights varies in the range of $\Delta h \approx 1\,300$–$1\,450$ nm. This is apparently due to the plasma-chemical and radiation effects on the copper foils, which usually oxidizes the boundaries of crystallites and remove material from the surface [6].

Only the surface of ME sample seven is characterized by notable smoothing (see Fig. 1, $Y \approx 6$ cm) where the roughness and height of the peaks fall pointwise to $S \approx 70$–100 nm and $\Delta h \approx 1\,000$–$1\,250$ nm, becoming comparable to the control sample. Electrons were apparently emitted precisely in the region where ME sample seven was taken. They heated the foil to the melting temperature locally and burned out peaks formed by radiation erosion [11, 12]. Analysis of the pore space of ME sample seven confirmed this assumption. Number n of pores in two areas (30×30 μm^2) of AFM scanning of the sample almost doubles (from $n = 768$ to $n = 1\,327$), indicating high heterogeneity of surface erosion according to the type of blistering. The AFM scanning revealed a porous surface in the area with the most intense formation of pores, on which blisters could no longer form [13].

The AFM revealed new structural effects that could result in the spontaneous emission of electrons in the MWPCs. It was found that nanoscale carbon films are formed in the cavities and interstructural spaces of the copper foil of ME samples. Figure 4 (*upper part*) shows a fragment of an AFM scan of ME sample eight with a graphite-like film ~ 20 nm thick. The film is inside a cavity on the surface and has a characteristic structure similar to images of nanographite films obtained under laboratory conditions by condensing carbon from the gas phase [12]. Figure 4 (*lower part*) shows the current-voltage characteristic measured in the area where nanographite film is formed. A current-voltage characteristic with voltage U rising from −10 to +10 V is indicated by *red dots*. A current-voltage characteristic with voltage U falling from +10 to −10 V is shown by *blue dots*. The current hysteresis displays resistive switching, which is typical of many nanocarbon formations. The threshold value of the electric field strength for the emission of electrons in such structures is $E_t \approx 10$ kV · cm^{-1} [14].

A nanocarbon film is uncontrollably and slowly formed on the copper foil of the MWPC cathode. This occurs in the electric field of the detector ($E_{\text{cathode}} \approx 5$ kV · cm^{-1}) with the gas mixture of $Ar/CO_2/CF_4$ at atmospheric pressure under prolonged exposure by the charged particles and processes of plasma-chemistry

interaction between the active radicals, ions, and copper. With AFM scanning, zones with a nanocarbon film are most often found near the walls of craters at the cathode.

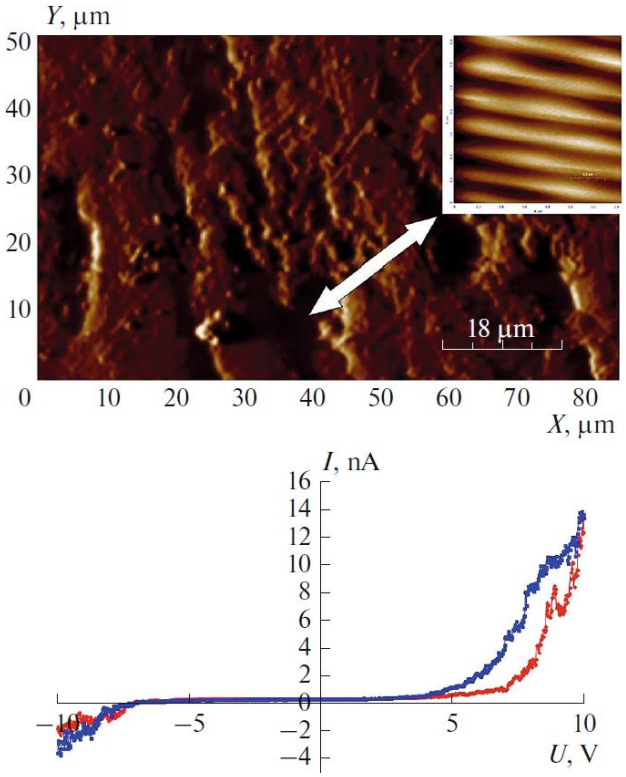

Fig. 4. An atomic force microscopy scan of ME sample eight with a scanning field size of 90 × 90 μm^2 (inset, 1.5 × 1.5 μm^2) is shown at the *top*. The current-voltage characteristic measured in the area of the nanographite film is shown *below*. The current-voltage characteristic upon raising voltage U from −10 to +10 V is represented by *red dots*. The current-voltage characteristic upon lowering voltage U from +10 to −10 V is given by *blue dots*

Our structural AFM-analysis of the MWPC cathode samples thus showed that the non-ME samples were characterized by a cellular structure with local zones of erosion. Radiation erosion was more pronounced in the ME samples. They were structurally heterogeneous, and their surfaces were smoothed as a result of melting. There were cascades of small craters (see Fig. 2*e*), and porous zones with many clearly visible small peaks and blisters. Nanosized carbon films were found at the boundaries of smoothed areas with loose defective areas, and in the cavities between microfibers in the ME samples. The observed morphological types of the surface were due to structural phase transformations and thermal processes that occurred on cathode surfaces under the action of charged particles and in pointwise zones of electron emission [12].

Integrated Rutherford backscattering spectra (RBSes) were analysed layer-by-layer for all types of the samples in areas of 300 × 300 μm^2. The depth of penetration measured for oxygen and carbon in the samples was no greater than 2 μm. The content of oxygen in near-surface layers (≤ 0.4 μm) was comparable for ME (~ 70%) and non-ME samples (~ 80%). On the other hand, the content of carbon in the ME samples (~ 15%) was three times higher than that in the non-ME samples (~ 5%). Graphite-like film formations on the surfaces of the ME samples are explained by their elevated carbon content (see Fig. 4). Another important difference between the samples was the presence of fluorine. In the RBS spectra of the ME samples, we detected fluorine at a level of ~ 5% in addition to carbon and oxygen, due to the high sensitivity of the procedure. We may therefore assume there were structures that contained fluorocarbon compounds CF_n on both cathodes surfaces in the MWPC.

Our results from studying samples *via* Raman spectroscopy were in good agreement with those from *X*-ray phase analysis. The oxide phase of Cu_2O and the phase of amorphous carbon were revealed on the analysed ME and non-ME surfaces by blowing the gas mixture through all four planes of the MWPC in succession. The gas flow thus redistributed active radicals in the working volume of the MWPC over all of the cathodes [2]. The presence of the Cu_2O oxide phase on the surface of the cathode in the MWPC of the LHCb muon detector agrees with results from studying detector prototypes. Laboratory tests of the MWPC

prototypes with an $Ar / CO_2 / CF_4$ gas mixture have also established that Cu_2O was the main phase of the surface layers of cathode samples [6].

Copper oxide is a *p*-type semiconductor and, like all semiconductor materials, it is sensitive to the presence of defects and microimpurities. They result in local energy levels emerging in the bandgap and changes in such conductivity parameters as the concentration and mobility of carriers. The presence of Cu_2O oxide microgranules on the cathode surface may be the reason for the appearance of many centres of electron and photon emission with a wavelength $\lambda \approx 600$ nm at the electric field above a threshold of $E_t \geq 50$ kV · cm^{-1} [8]. Due to the absorption of electrons in a cathode's material, however, the emission of electrons into the gas volume of the detector becomes impossible at a depth of ~ 1 μm. From the experience of observing ME in gas-discharge detectors, it is known that the dielectric on the cathode surface should be no more than several tens of nanometers thick for emission currents to appear [7]. Spontaneous currents due to Cu_2O granules are possible in the MWPC only if they form on the surface of a cathode in the form of micropeaks with an aspect factor (ratio of the height to the tip diameter) greater than 10 for the electric field on the cathode ($E_{\text{cathode}} \approx 5$ kV · cm^{-1}). The current of electrons through such a microobject heats the foil up to the melting point (T_{Cu_2O} = 1 235°C). The emission of electrons stops as a result of changes in the electrochemical properties of the material. The next possible reason for the ME is the emission of electrons by nanographite structures. The results revealed the condensation of carbon- and fluorine containing molecules on the cathode that were produced in the gas-discharge plasma near the anode wire. An example of such structures are nanographite films that form crystallites 1–2 μm tall. Since they are thin, the aspect ratios of these structures can be as great as 1 000. The threshold value of the electric field for electron emission by nanographite films is $E_t \approx 10$ kV · cm^{-1}. This value of the electric field strength is easily achievable in an MWPC [11, 12].

The presence of fluorine and nanocarbon on the cathode surface can result in the formation of dielectric fluorocarbon compounds, which are a stable source of emission currents [14]. It is difficult to attribute definitely the nanostructures observed in the MWPC to one of the many models of low-threshold emission. To identify the reasons for the ME, however, it is important that almost all such nanostructures are characterized by electron emission.

4. Conclusion

The surface of a MWPC cathode from the LHCb experiment at the LHC was studied comprehensively for the first time in order to establish the reasons for spontaneous self-sustaining currents in the detector. Radiation erosion accompanied by the formation of copper oxide and nanosized carbon and fluorocarbon structures of high resistivity were revealed by the AFM, microprobes, *X*-ray diffractometry and Raman spectroscopy on the copper foil of the cathode. A characteristic feature of carbon and fluorocarbon nanostructures is the low threshold of electron emission. The threshold value of the electric field strength for nanostructures ($E_t \sim 10$ kV · cm^{-1}) is one fifth that of Cu_2O, and it can be reached on a cathode under the conditions of radiation damaging copper. Carbon and fluorocarbon nanostructures therefore seem to be the most realistic source of spontaneous currents in the MWPC.

References

1. L. Malter, Phys. Rev. **50**, 48 (1936).
2. F.P. Albicocco, L. Anderlini, M. Anelli *et al*., JINST **14**, P11031 (2019).
3. H.H. Hansen, Int. J. Appl. Radiat. Isot. **34**, 1241 (1983).
4. S.B. Fisher, Radiat. Eff. Defects Solids **7**, 173 (1971).
5. D. Pfeiffer, G. Gorine, *et al*., Nucl. Instrum. Meth. Phys. Res., Sect. A, **866**, 91 (2017).
6. M.E. Buzoverya, G.E. Gavrilov, O.E. Maev, Tech. Phys. **66** (2), 356 (2021).
7. G. Zhou, L. Wang, J.C. Yang, J. Appl. Phys. **97**, 063509 (2005).
8. R.E. Hurley, J. Phys. D: Appl. Phys. **10**, L195 (1979).
9. J. Va'Vra, Nucl. Instrum. Meth. Phys. Res., Sect. A **252**, 547 (1986).
10. V.A. Akat'ev, E.V. Metelkin, At. Energy **118** (2), 105 (2015).

11. A.N. Obraztsov, Al.A. Zakhidov, Diamond Relat. Mater. **13**, 1044 (2004).
12. A.N. Obraztsov, V.I. Kleshch, J. Nanoelectron. Optoelectron. **4**, 207 (2009).
13. M.I. Guseva, Yu.V. Martynenko, Sov. Phys. Usp. **24**, 996 (1981).
14. A.I. Ivanov, N.A. Nebogatikova, I.I. Kurkina, I.V. Antonova, Semiconductors **51** (10), 1306 (2017).